Research Article

Meirong Ren, Tiange Zhang, Jifeng Cui, Xiaogang Chen*, and Bixia Wu

Magnetofluid unsteady electroosmotic flow of Jeffrey fluid at high zeta potential in parallel microchannels

https://doi.org/10.1515/phys-2022-0051
received March 04, 2022; accepted May 24, 2022

Abstract: In this article, the magnetofluid unsteady electroosmotic flow (EOF) of Jeffrey fluid with high zeta potential is studied by using the Chebyshev spectral method and the finite difference method. By comparing the potential distribution and velocity distribution obtained by the Chebyshev spectral method and finite difference method, it is concluded that the Chebyshev spectral method has higher precision and less computation. Then the numerical solution obtained by the Chebyshev spectral method is used to analyze the flow characteristics of Jeffrey fluid at high zeta potential. The results show that the velocity of Jeffrey fluid increases with the increase of the wall zeta potential and electric field intensity. The oscillation amplitude of velocity distribution increases with the increase of relaxation time, but decreases with the increase of retardation time. With the increase of Hartmann number, the velocity first increases and then decreases. The positive pressure gradient promotes the flow of fluid, and the reverse pressure gradient impedes the flow of fluid.

Keywords: magnetohydrodynamics, EOF, electric double layer, Jeffrey fluid, parallel plate microtube

1 Introduction

With the rapid development of modern science and technology in the microscale and nanoscale, the research related to the microscale and nanoscale transport has developed rapidly. This brings about a fundamental technological change to the miniaturization of analytical devices. Currently, transport processes at the microscale and nanoscale include microelectro-mechanical systems, drug delivery and control of microelectronic devices and so on. First, people used the traditional pressure drive to drive the flow in the microscale and nanoscale pipelines, but people gradually realized that the flow at microscale has completely different characteristics from the flow at macroscale. Therefore, electroosmosis drive becomes an effective and feasible new option. It is more and more concerned by researchers for its advantages of simple operation, high reliability, and easy control. It is widely used in microfluidic systems, DNA detection, transportation, and separation. Up to now, scholars at home and abroad have made abundant achievements on electroosmotic drive in microchannels [1–7].

However, electroosmotic drive has its own disadvantages, and it is limited to the delivery of a small amount of liquid sample in the microfluidic device. Therefore, the external magnetic field or electric and magnetic field hybrid drive mode is more and more introduced into microfluidic devices to further improve the efficiency and function of the microscale and nanoscale devices. Magnetohydrodynamic (MHD) [8] has a wide range of applications in modern industry, including bubble levitation, alloy manufacture, nuclear heat transfer control, etc. So far, there have been a lot of relevant research achievements. For example, Shamshuddin and Ibrahim [9] applied the Buongiorno nanofluid model to study the steady-state electromagnetic fluid flow of micropolar nanofluids when a reactive Carson fluid passes through a parallel plate affected by a rotating system; Shahid *et al.* [10] scrutinized the incompressible steady flow with temperature-dependent viscosity of magnetohydro-dynamics nanofluid through a vertically stretched porous sheet and so on. To obtain higher fluid velocity, people began to consider electroosmotic drive and electromagnetic drive together. In general, the problem of microfluidic flow coupled with electric field, magnetic field, and electric

* **Corresponding author: Xiaogang Chen,** College of Science, Inner Mongolia University of Technology, Hohhot 010051, China, e-mail: xiaogang_chen@imut.edu.cn
Meirong Ren, Tiange Zhang, Jifeng Cui, Bixia Wu: College of Science, Inner Mongolia University of Technology, Hohhot 010051, China

double layer effect is called magnetohydrodynamic electroosmotic flow. Chakraborty and Paul [11] took account of the combined influences of electromagnetohydrodynamic forces in controlling the fluid flow through parallel plate rectangular microchannels; Ganguly *et al.* [12] delineated the heat transfer characteristics of thermally developing magnetohydroclynamic flow of nanofluid through microchannel by following a semi analytical approach; Zhao *et al.* [13] investigated the heat transfer characteristics of thermally developed nanofluid flow through a parallel plate microchannel under the combined influences of externally applied axial pressure gradient and transverse magnetic fields; Das *et al.* [14] presented a generic framework for describing the flow field that is generated under the combined influences of a driving pressure gradient, an axial electric field, and a spatially varying transverse magnetic field. The unsteady electroosmosis, pressure-driven, and MHD flow of conductive, incompressible, and viscous fluid through a parallel plate microchannel with a vertical magnetic field has been studied by using the Laplace transform method by Jian [15]; Wang [16] studied the electroosmotic flow (EOF) of Jeffrey fluid in parallel plate micropipes under vertical magnetic field by using the separation transformation method; Yang [17] studied the flow, heat transfer, and entropy generation of three grade fluid in parallel plate and so on.

All the studies mentioned earlier are about the flow of micro-nano fluids in micropipes under low zeta potential, but in practical application, the wall zeta potential of most interfaces is higher than 25 mV. Therefore, many scholars have studied the flow of micro-nano fluids in micropipes under high zeta potential. By using the method of separation of variables, Liu *et al.* [18] studied the time periodic EOF flow of linear viscoelastic fluids between micro-parallel plates, and semi-analytical solutions are presented; Qi *et al.* [19] studied the electroosmotic flow of fractional Maxwell fluid in rectangular microchannels with high zeta potential; Vasu and De [20] investigated the electroosmotic flow of the power-law fluid under high zeta potential in a cylindrical microcapillary for different dimensionless parameters; rotating EOF of power-law fluids at high zeta potentials in a slit microchannel is analyzed by Xie and Jian *et al.* [21], and the finite difference method is used to compute numerically rotating EOF velocity profiles of power-law fluids; Chang and Jian [22] investigated the periodic electroosmotic flow of linear viscoelastic fluid in two parallel plate microtubes with high zeta potential; Chen and Liu [23] investigated the rotational electroosmotic flow of Newtonian fluid in parallel microchannels with high zeta potential and so on.

The non-Newtonian fluid has a great importance owing to its practical usefulness as related to science, engineering, and industrial applications [24,25]. Its physical properties and complex rheological properties can be explained by constitutive relation [26]. The Jeffrey fluid model is an important extension of the Newtonian fluid model and can be derived as a special case of the non-Newtonian fluid model [27]. One of its important application is to represent a physiological fluid. Up to now, many studies have been conducted on the flow properties of Jeffrey fluid in microtubes. For instance, Shahzad *et al.* [28] analyzed the magnetohydrodynamics heat act of a viscous incompressible Jeffrey nanoliquid, which passed in the neighborhood of a linearly extending foil; Li *et al.* [29] investigated the time-periodic pulse EOF of Jeffrey fluid through a microannulus by using the Laplace transform method; Gireesha *et al.* [30] investigated the three-dimensional boundary layer radiative flow with thermophoresis and Brownian motion for Jeffrey fluid over a nonlinearly permeable stretching sheet and discussed the influence of nonlinear thermal radiation on magnetohydrodynamic three-dimensional boundary layer flow and so forth. But there are few studies on the flow characteristics of Jeffrey fluid in different microtubes at high zeta potential.

The main purpose of this article is to further study the magnetofluid unsteady electroosmotic flow of Jeffery fluid in parallel microtubes at high zeta potential. Firstly, the finite difference method and Chebyshev spectral method are used to solve the nonlinear P–B equation, and the numerical solution of the potential distribution is obtained. Second, for the solution of the velocity distribution, we also adopt the aforementioned two kinds of methods to solve the Cauchy momentum equation. In addition, we use fourth-fifth order Runge–Kutta algorithm to deal with time variable. Finally, the numerical solutions obtained by the aforementioned two methods are compared with the asymptotic analytical solution obtained by Debye–Hückel linear approximation. The influence of various physical parameters on velocity distribution is given and discussed in detail.

2 Mathematical model

As shown in the Figure 1, considering the magnetohydrodynamic unsteady EOF of the incompressible Jeffrey fluid in the negatively charged parallel microchannel with a distance of $2h$ between the two plates, that is, the length of the microchannel is L and the width is W, it is assumed that these two parameters are much greater than the height of the microchannel, that is, $L \gg W \gg 2h$. A space

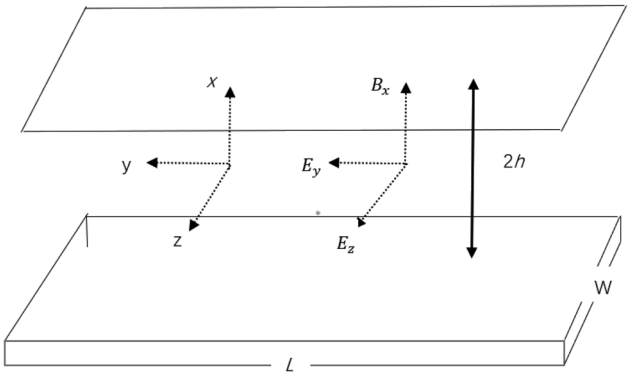

Figure 1: Schematic diagram of Jeffrey fluid flow in parallel microchannel.

rectangular coordinate system is established, in which the y-axis direction is the flow direction, the x-axis is perpendicular to the charged surface, and points out from the flow surface along the z-axis. At the same time, we stipulate that the lower plate is at $x = -h$ and the upper plate is at $x = h$. It is assumed that the fluid is subjected to both electric field $\boldsymbol{E} = (0, E_y, E_z)$ and magnetic field $\boldsymbol{B} = (B_x, 0, 0)$. The density, viscosity, and conductivity of the fluid are ρ, μ, σ_e. The chemical interaction between the electrolyte solution and the solid wall produces electric double layer (EDL). Electric field in the axial direction of the pipe. Under the action of E_y, the ions in EDL will move. Under the action of the viscous force of the ions, the movement of the ions drives the fluid to move together. In addition, the Lorentz force generated by the magnetic field and pressure gradient are also another driving force of the fluid movement.

3 Formula derivation

3.1 Potential distribution

According to the electrostatic theory, the relationship between electric potential $\overline{\psi}$ and electrostatic charge density per unit volume ρ_e can be described by the following Poisson–Boltzmann equation:

$$\nabla^2\overline{\psi} = -\frac{\rho_e}{\varepsilon}, \tag{1}$$

where ε is the dielectric constant.

The ion concentration per unit volume of electrolyte solution obeys Boltzmann distribution as follows:

$$n_v = n_{v0}\exp\left(-\frac{z_v e\overline{\psi}}{k_b T}\right), \tag{2}$$

where z_v is the ionic valence of the ion, n_{v0} is the ionic concentration of the electrolyte solution, e is the amount of charge carried by the electron, T is the absolute temperature, and k_b is the Boltzmann constant.

Electrostatic charge density per volume ρ_e is expressed as follows:

$$\rho_e = \sum n_v z_v e = e\sum z_v n_{v0}\exp\left(-\frac{z_v e\overline{\psi}}{k_b T}\right), \tag{3}$$

for solution $z_+ : z_- = 1:1$, Eq. (3) is specifically

$$\rho_e = -2n_0 z_v e\sinh\left(-\frac{z_v e\overline{\psi}}{k_b T}\right). \tag{4}$$

By substituting Eq. (2) into Eq. (1), the Poisson–Boltzmann equation satisfied by the electric potential $\overline{\psi}$ is obtained as follows:

$$\nabla^2\overline{\psi} = \frac{\mathrm{d}^2\overline{\psi}}{\mathrm{d}\overline{x}^2} = \frac{2n_0 z_v e}{\varepsilon}\sinh\left(\frac{z_v e\overline{\psi}}{k_b T}\right), \tag{5}$$

and the boundary condition is expressed as follows:

$$\overline{\psi}(\overline{x})|_{\overline{x}=h} = \overline{\psi}_0,\ \frac{\mathrm{d}\overline{\psi}(\overline{x})}{\mathrm{d}\overline{x}}\bigg|_{\overline{x}=0} = 0, \tag{6}$$

where $\kappa = (2n_0 z_v^2 e^2/\varepsilon k_b T)^{1/2}$, $\overline{\psi}_0$ is wall zeta potential, and κ is called Debye–Hückel parameter, whose reciprocal $1/\kappa$ representing the thickness of EDL is called Debye length.

The following dimensionless variables are introduced:

$$x = \frac{\overline{x}}{h},\ (\psi, \psi_0) = \frac{z_v e}{k_b T}(\overline{\psi}, \overline{\psi}_0),\ K = \kappa h. \tag{7}$$

By substituting the aforementioned dimensionless variables into Eqs. (5) and (6), the dimensionless equation and boundary conditions of potential distribution can be obtained as follows:

$$\frac{\mathrm{d}^2\psi}{\mathrm{d}x^2} = K^2\sinh(\psi), \tag{8}$$

$$\psi(x)|_{x=1} = \psi_0,\quad \frac{\mathrm{d}\psi(x)}{\mathrm{d}x}\bigg|_{x=0} = 0. \tag{9}$$

3.2 Velocity distribution

The velocity of the fluid satisfies the following continuity equation and Cauchy momentum equation:

$$\nabla\cdot\boldsymbol{u} = 0, \tag{10}$$

$$\rho(\partial\boldsymbol{u}/\partial t + (\boldsymbol{u}\cdot\nabla)\cdot\boldsymbol{u}) = -\nabla p - \nabla\cdot\tau + \boldsymbol{f}, \tag{11}$$

where $\boldsymbol{u}$ is the fluid velocity, t is the time, p is the pressure, and $\boldsymbol{f}$ is the volume force, which is equal to the sum

of the electric field force $\rho_e(x)\boldsymbol{E}$ and the Lorentz force $\boldsymbol{J}\times\boldsymbol{B}$,

$$\boldsymbol{f}=\rho_e(x)\boldsymbol{E}+\boldsymbol{J}\times\boldsymbol{B}, \tag{12}$$

and here, the current $\boldsymbol{J}$ satisfies Ohm's law:

$$\boldsymbol{J}=\sigma_e(\boldsymbol{E}+\boldsymbol{u}\times\boldsymbol{B}). \tag{13}$$

The final simplified transient momentum conservation equation along the y direction can be expressed in the following form:

$$\rho\frac{\partial\overline{u}}{\partial\overline{t}}=-\frac{\mathrm{d}p}{\mathrm{d}y}-\frac{\partial\overline{\tau}_{\overline{xy}}}{\partial\overline{x}}+\rho_eE_y,$$
$$+\sigma_eE_zB_x-\sigma_eE_zB_x^2\overline{u}. \tag{14}$$

The component $\overline{\tau}_{\overline{xy}}$ of shear stress tensor satisfies the constitutive equation of Jeffrey fluid [31]:

$$\left(1+\overline{\lambda}_1\frac{\partial}{\partial\overline{t}}\right)\overline{\tau}_{\overline{xy}}=-\eta_0\left(\frac{\partial\overline{u}}{\partial\overline{x}}+\overline{\lambda}_2\frac{\partial^2\overline{u}}{\partial\overline{t}\partial\overline{x}}\right). \tag{15}$$

The velocity satisfies the following initial and boundary conditions:

$$\overline{u}\,|_{\overline{t}=0}=0,\ \left.\frac{\partial\overline{u}}{\partial\overline{t}}\right|_{\overline{t}=0}=0, \tag{16}$$

$$\overline{u}\,|_{\overline{x}=h}=0,\ \left.\frac{\partial\overline{u}}{\partial\overline{x}}\right|_{\overline{x}=0}=0. \tag{17}$$

The following dimensionless variables are introduced:

$$u=\frac{\overline{u}}{v_{\mathrm{HS}}},\ (t,\lambda_1,\ \lambda_2)=\frac{(\overline{t},\overline{\lambda}_1,\overline{\lambda}_2)}{\rho h^2/\eta_0}, \tag{18}$$

$$\mathrm{Ha}=B_xh\sqrt{\frac{\sigma_e}{\eta_0}},\ \beta=\frac{E_zh}{v_{\mathrm{HS}}}\sqrt{\frac{\sigma_e}{\eta_0}}, \tag{19}$$

$$v_{\mathrm{HS}}=-\frac{\varepsilon k_bTE_y\psi_0}{z_0e\eta_0},\ \tau_{xy}=\frac{\overline{\tau}_{\overline{xy}}}{\eta_0v_{\mathrm{HS}}/h}, \tag{20}$$

where Ha is Hartmann number, which is a parameter to measure the ratio of magnetic force to viscous force. K is a dimensionless electric width, β is dimensionless parameter representing the electric field intensity in the z axial direction, and v_{HS} represents the Helmholtz–Smoluchowski electroosmotic velocity.

By introducing Eqs. (17)–(19) into Eqs. (14)–(16), the dimensionless equation and boundary value condition of velocity distribution can be obtained:

$$\lambda_1\frac{\partial^2u}{\partial t^2}+(1+\lambda_1\mathrm{Ha}^2)\frac{\partial u}{\partial t}=\Omega+\lambda_2\frac{\partial^3u}{\partial t\partial x^2}+\frac{\partial^2u}{\partial x^2}$$
$$+\frac{K^2\sinh\psi}{\psi_0}+\beta\mathrm{Ha}-\mathrm{Ha}^2u, \tag{21}$$

$$u\,|_{t=0}=0,\ \left.\frac{\partial u}{\partial t}\right|_{t=0}=0, \tag{22}$$

$$u\,|_{x=1}=0,\ \left.\frac{\partial u}{\partial x}\right|_{x=0}=0, \tag{23}$$

where $\frac{\mathrm{d}p}{\mathrm{d}z}=-\frac{\Delta p}{L}$, $\Omega=\frac{v_p}{v_{\mathrm{HS}}}$ is the ratio of axial pressure gradient velocity to electroosmosis driving velocity, and v_p is the flow velocity driven by axial pressure, which can be expressed as $v_p=\Delta ph^2/\eta_0L$.

4 Numerical method

The finite difference method is a local method in which the derivative at each point is calculated from several adjacent points, so the matrix used in the calculation is a sparse matrix with many zeros; and therefore, its accuracy is relatively low [32]. The Chebyshev spectral method is a global algorithm, which uses all known points to calculate the derivative of a certain point, greatly improving the accuracy [32].

4.1 Potential distribution

4.1.1 Chebyshev spectral method

We first select the Chebyshev point defined in $(-1, 1]$ [33]:

$$x_p=-\cos((j\pi)/N),\ p=0,\ldots,N. \tag{24}$$

Let $\psi=[\psi(x_0),\psi(x_1),\ \ldots,\psi(x_N)]$ be the undetermined vector on the Chebyshev point, and then we obtained a Chebyshev polynomial $P(x)$, i.e., $P(x_i)=\psi(x_i)$, $i=0,1,\ldots,N$. By deriving $P(x_i)$ and evaluating it at the grid point, we can transform the differential equation into a linear algebraic equation. Finally, the numerical solution of dimensionless potential distribution is obtained by the Newton iterative method under conditional formula.

4.1.2 Finite difference method

Let $\Delta h=1/N$, $i=1\sim(N-1)$, the central difference of the above formula is obtained:

$$\frac{1}{h^2}(\psi_{(i+1)}-2\psi_{(i)}+\psi_{(i-1)})-K^2\sinh\psi_{(i)}=0. \tag{25}$$

The discrete format equation of the corresponding initial and boundary conditions is expressed as follows:

$$\psi_{(1)}=\psi_{(0)},\ \psi_{(N)}=\psi_0. \tag{26}$$

4.1.3 Comparison of results

The results obtained by the Chebyshev spectral method and the finite difference method are compared with the D–H linear approximate analytical solution, as shown in Figure 2. Under the low zeta potential, when the number of points is small (8 points in Figure 2(a)), the accuracy of the finite difference method is poor, while the Chebyshev spectral method only needs a few points to achieve high accuracy. Under the high zeta potential, when the number of points of the finite difference method reaches 100 (see Figure 2(b)). The Chebyshev spectral method only takes a few points (30 points in Figure 2(b)), and the two curves can be consistent. The results show that the Chebyshev spectral method has higher accuracy and less computation than the finite difference method.

4.2 Velocity distribution

4.2.1 Chebyshev spectral method

Introduce the function $v(r, t) = \partial u(r, t)/\partial t$ and reduce $\partial^2/\partial t^2$ in Eqs. (20) and (21) to $\partial/\partial t$, and we obtain

$$\begin{cases} \dfrac{\partial u}{\partial t} = v, \\ \dfrac{\partial v}{\partial t} = \dfrac{1}{\lambda_1}\left[\lambda_2\dfrac{\partial^2 v}{\partial x^2} + \dfrac{\partial^2 u}{\partial x^2} - \mathrm{Ha}^2 u - (1+\lambda_1\mathrm{Ha}^2)v + \Omega \right. \\ \qquad \left. + \beta\mathrm{Ha} + \dfrac{K^2\sinh(\psi)}{\psi_0}\right], \\ u|_{t=0} = 0, v|_{t=0} = 0, \\ u|_{x=-1} = 0, u|_{x=1} = 0, \\ v|_{x=-1} = 0, v|_{x=1} = 0. \end{cases} \tag{27}$$

We use the derivative matrix of Chebyshev–Spectral to compute the derivative in the x direction and use fourth-fifth order Runge–Kutta algorithm (ode45) to calculate $\partial/\partial t$ in Eq. (27) [34].

4.2.2 Finite difference method

Let $\Delta h = 1/N$, $\Delta t = 1/M$, $j = 1 \sim (N-1)$, $k = 1 \sim (M-1)$, and write the aforementioned formula as the central difference scheme, and we obtain

$$\begin{aligned} &\left(\frac{\lambda_1}{\Delta t^2} + \frac{1+\lambda_1\mathrm{Ha}^2}{2\Delta t} + \frac{\lambda_2}{\Delta h^2\Delta t}\right)u_j^{k+1} - \frac{\lambda_2}{\Delta h^2\Delta t}u_{j+1}^{k+1} - \frac{\lambda_2}{\Delta h^2\Delta t}u_{j-1}^{k+1} \\ &= \frac{1}{\Delta h^2}u_{j-1}^{k} + \frac{1}{\Delta h^2}u_{j+1}^{k} - \left(\mathrm{Ha}^2 + \frac{2}{\Delta h^2} - \frac{2\lambda_1}{\Delta t^2}\right)u_j^{k} \\ &\quad + \left(\frac{1+\lambda_1\mathrm{Ha}^2}{2\Delta t} + \frac{\lambda_2}{\Delta h^2\Delta t} - \frac{\lambda_1}{\Delta t^2}\right)u_j^{k-1} - \frac{\lambda_2}{\Delta h^2\Delta t}u_{j+1}^{k-1} \\ &\quad - \frac{\lambda_2}{\Delta h^2\Delta t}u_{j-1}^{k-1} + \Omega + \beta\mathrm{Ha} + \frac{K^2}{\psi_0}\sinh\psi_j. \end{aligned} \tag{28}$$

4.2.3 Comparison of results

The numerical solution of dimensionless velocity distribution obtained by the Chebyshev spectral method and the finite difference method is compared with the velocity distribution obtained by D–H linear approximation under low zeta potential, as shown in Figure 3(a). We can see that taking a small number of points (8 points in Figure 3(a)), the Chebyshev spectral method has higher accuracy than the finite difference method. At high zeta potential (Figure 3(b)), it can also be noted that when enough points (100 points in Figure 3(b)) are taken for the finite difference method, the velocity curve

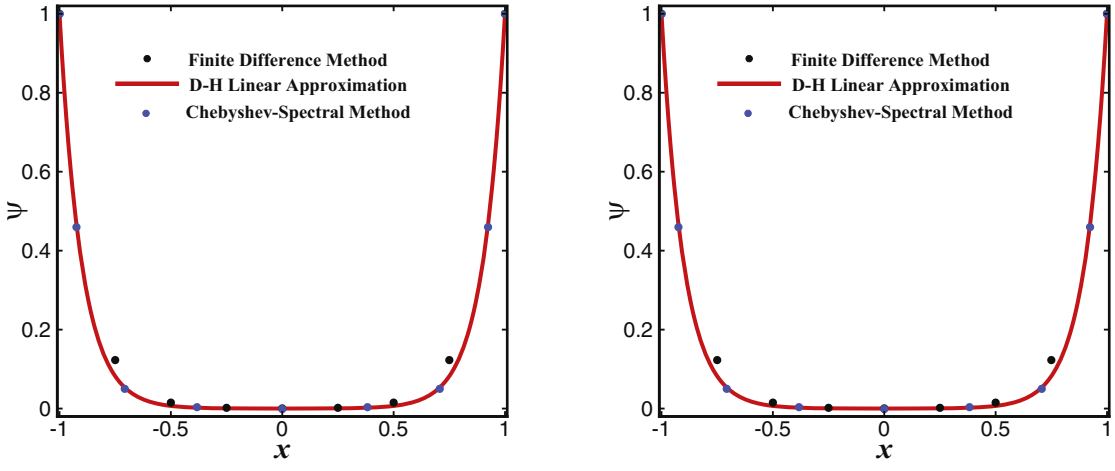

Figure 2: Comparison of the Chebyshev spectral method with finite difference numerical solution and D–H linear approximate analytical solution for solving nonlinear P–B equations ($K = 20$). (a) $\psi_0 = 1$ and (b) $\psi_0 = 10$.

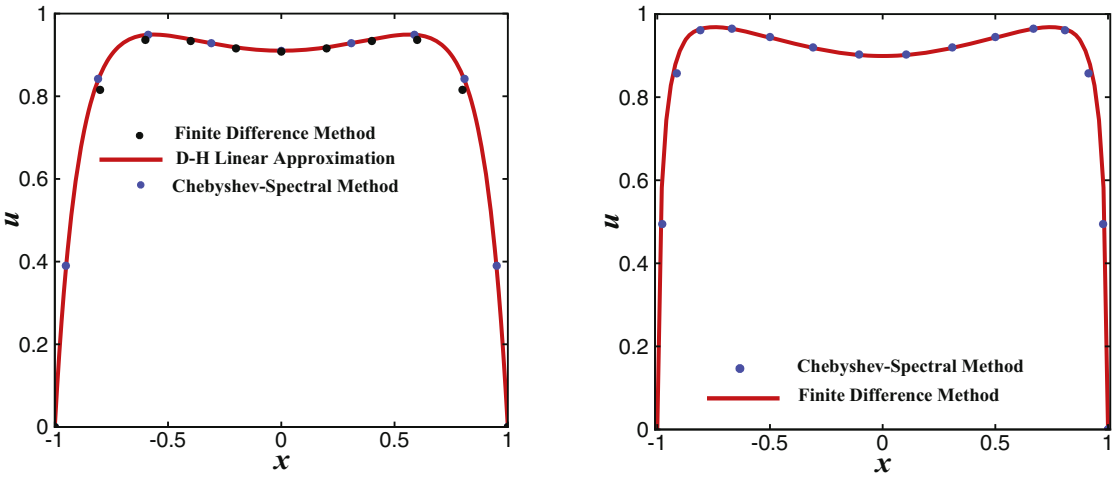

Figure 3: Comparison of velocity profiles among the Chebyshev spectral method, finite difference method and D–H linear approximate analytical solution (K = 20, Ω = 1, Ha = 1, β = 1, λ_1 = 0.8, λ_2 = 0.3, t = 1). (a) ψ_0 = 1 and (b) ψ_0 = 10.

solved by the finite difference method can be relatively consistent with that solved by the Chebyshev spectral method (30 points in Figure 3(b)). Therefore, the velocity distribution obtained by the Chebyshev spectral method is more accurate and less computational than that obtained by the finite difference method. It is feasible to extend the Chebyshev spectral method to solve the velocity distribution of fluid under high zeta potential.

5 Discussion

In this article, the magnetohydrodynamic unsteady electroosmotic flow of Jeffrey fluid in parallel plate microchannels under high zeta potential is studied, and the numerical solution of velocity distribution is obtained, which is mainly determined by several dimensionless parameters (Table 1), such as Hartmann number Ha, Jeffrey fluid relaxation time λ_1 and retardation time λ_2, ratio Ω of velocity amplitude to axial applied pressure gradient and electroosmotic driving velocity, dimensionless time t, and dimensionless electric field intensity in z axial direction β. We will mainly discuss the influence of the above parameters on velocity amplitude. In the following calculation, typical parameter values are as follows [16]: h = 200 μm, $\rho = 10^3$ kg m^{-3}, $\eta_0 = 10^{-3}$ kg m^{-1} s^{-1}, and $\sigma_e = 2.2 \times 10^{-4}$–$10^6$/m. If the range of magnetic field strength B_x is 0–0.44T [35], the range of Ha can be 0–5. Similarly, if the variation range of applied alternating electric field strength E_z is 0–1 V/m and v_{HS} = 100 μm/s, then the value range of the dimensionless parameter β is $0-6 \times 10^4$, and the retardation time should be less than the relaxation time.

Table 1: List of symbols

Symbol	Meaning
B	Magnetic field intensity (T)
e	The amount of charge an electron carries (C)
k_b	Boltzmann constant (J/K)
L	Microtube length (m)
W	Microtube width (m)
H	Microtube height (m)
Ha	Hartman constant
n_{v0}	Liquid ion concentration (l/mol)
p	Pressure (N)
β	Lateral electric field parameter (N)
t	Time (s)
T	Absolute temperature (T)
$\boldsymbol{u}$	Velocity vector (m/s)
σ	Electrical conductivity (S/m)
$\boldsymbol{\tau}$	The stress tensor
λ_1	Relaxation time (s)
λ_2	Retardation time (s)
η	Coefficient of viscosity (Pa s)
ρ_a	Electric density (C/m)
ε	Dielectric constant
κ	Debye–Hückel constant

The effects of different Hartmann number Ha and ψ_0 on the dimensionless velocity profile u are analyzed in Figure 4. It can be seen from the Figure 4 that the increase of wall zeta potential ψ_0 has a great influence on the velocity near the wall, that is, the greater the wall zeta

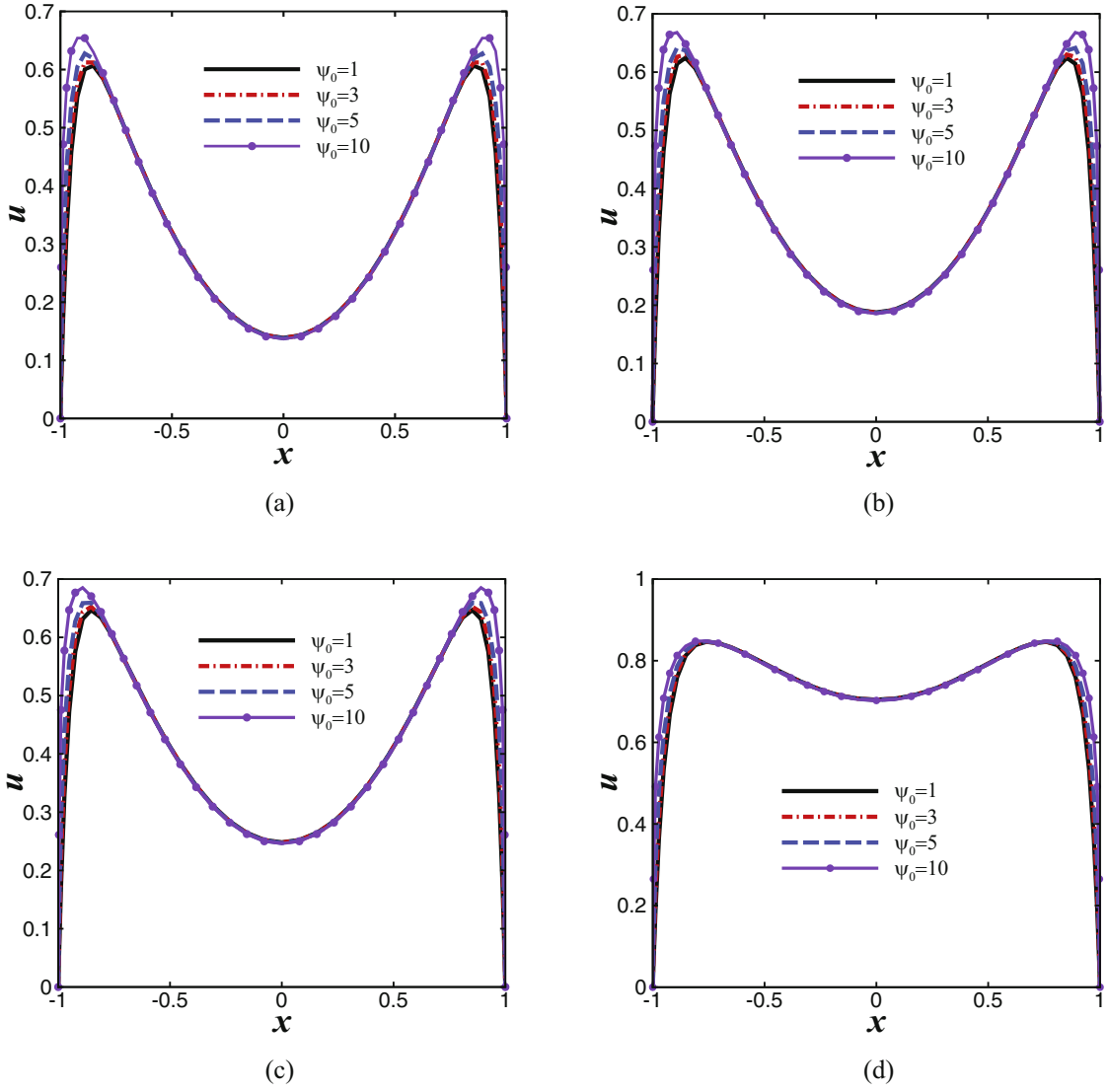

Figure 4: Effects of different Ha and ψ_0 on dimensionless velocity profiles u ($\lambda_1 = 0.8, \lambda_2 = 0.3, \Omega = 0, \beta = 10, K = 20, t = 0.5$). (a) Ha = 0.01, (b) Ha = 0.05, (c) Ha = 0.1, and (d) Ha = 0.5.

potential is, the greater the velocity u, and the maximum variation region of velocity u is limited to the thin layers of two solid surfaces, that is, EDL. The main reason is that the flow has no enough time to diffuse away from the wall, and when the value of Ha is small, electroosmotic force plays a leading role, so the wall zeta potential has a great influence on the velocity near EDL. The velocity profile u increases rapidly from zero to maximum in the EDL range, and the velocity shows a significant depression in the center of the pipe, which is caused by the interaction between the external drive and the EDL. Furthermore, when the zeta potential is constant, the velocity u increases with the increase of Ha (Ha < 1). Because with the increase of Ha, the Lorentz force increases and thus the velocity increases. In conclusion, both Hartmann number Ha and wall zeta potential ψ_0 have significant effects on the dimensionless velocity u.

The effect of Ha and ψ_0 on the dimensionless velocity profile u is analyzed in Figure 5. When Ha > 1, the velocity u decreases with the increase of Ha because the resistance part of Lorentz force increases with the increase of Ha. The total Lorentz force is much greater than the electroosmosis force, resulting in a decrease in velocity u. These findings are identical to the physical fact that an opposite direction force commonly called drag force, which is known as Lorentz force, which is created with the enhancement of magnetic parameter. It can also be seen from Figure 5 that the increase of wall zeta potential

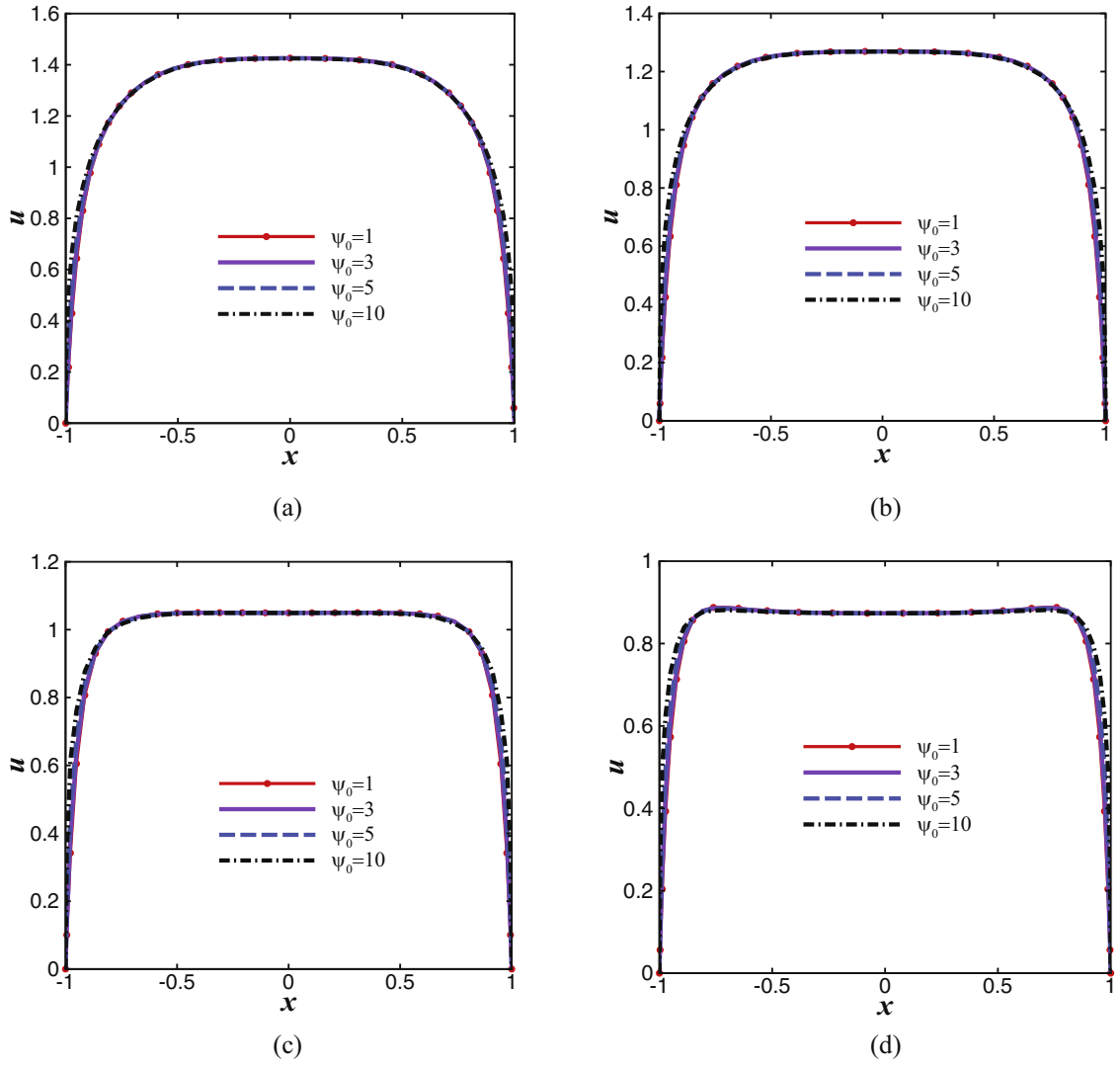

Figure 5: Effects of different Ha and ψ_0 on dimensionless velocity profiles u ($\lambda_1 = 0.8, \lambda_2 = 0.3, \beta = 10, \Omega = 0, K = 20, t = 0.5$). (a) Ha = 2, (b) Ha = 3, (c) Ha = 4, and (d) Ha = 5.

ψ_0 has a little influence on the velocity near the wall, and the maximum variation area of velocity u is limited to the thin layers of two solid surfaces, namely, EDL. The main reason is that the flow has no enough time to diffuse away from the wall. When the value of Ha is large, Lorentz force plays a leading role, so the wall zeta potential has a little effect on the velocity near EDL.

The effects of different β and ψ_0 on the dimensionless velocity profile u at $x = 0.95$ (i.e., EDL) are analyzed in Figure 6. It is clear from Figure 6 that when the zeta potential is constant, the flow velocity profile u increases with the increase of β. The increase of β means that the strength of the external electric field along the z axis increases, and thus, the Lorentz force driving the fluid increases. Thus, the flow velocity profile u increases as β increases. When β is constant, the velocity u in EDL increases with the increase of the wall zeta potential ψ_0. In conclusion, both β and the wall zeta potential ψ_0 have significant effects on the dimensionless velocity u.

Figure 7 analyzes the effects of different Ω and ψ_0 on the dimensionless velocity profile u in $x = 0.95$. It is easy to see from Figure 7 that the higher the forward pressure gradient is, the higher the velocity is, because when the pressure gradient is forward pressure gradient, the direction of the electroosmotic force, Lorentz force, and the forward pressure drive are the same, to facilitate the flow of fluids. In contrast, when a negative pressure gradient is applied, the direction of electroosmotic force and Lorentz force is opposite to the driving direction of reverse pressure, impeding the flow of the fluid, and

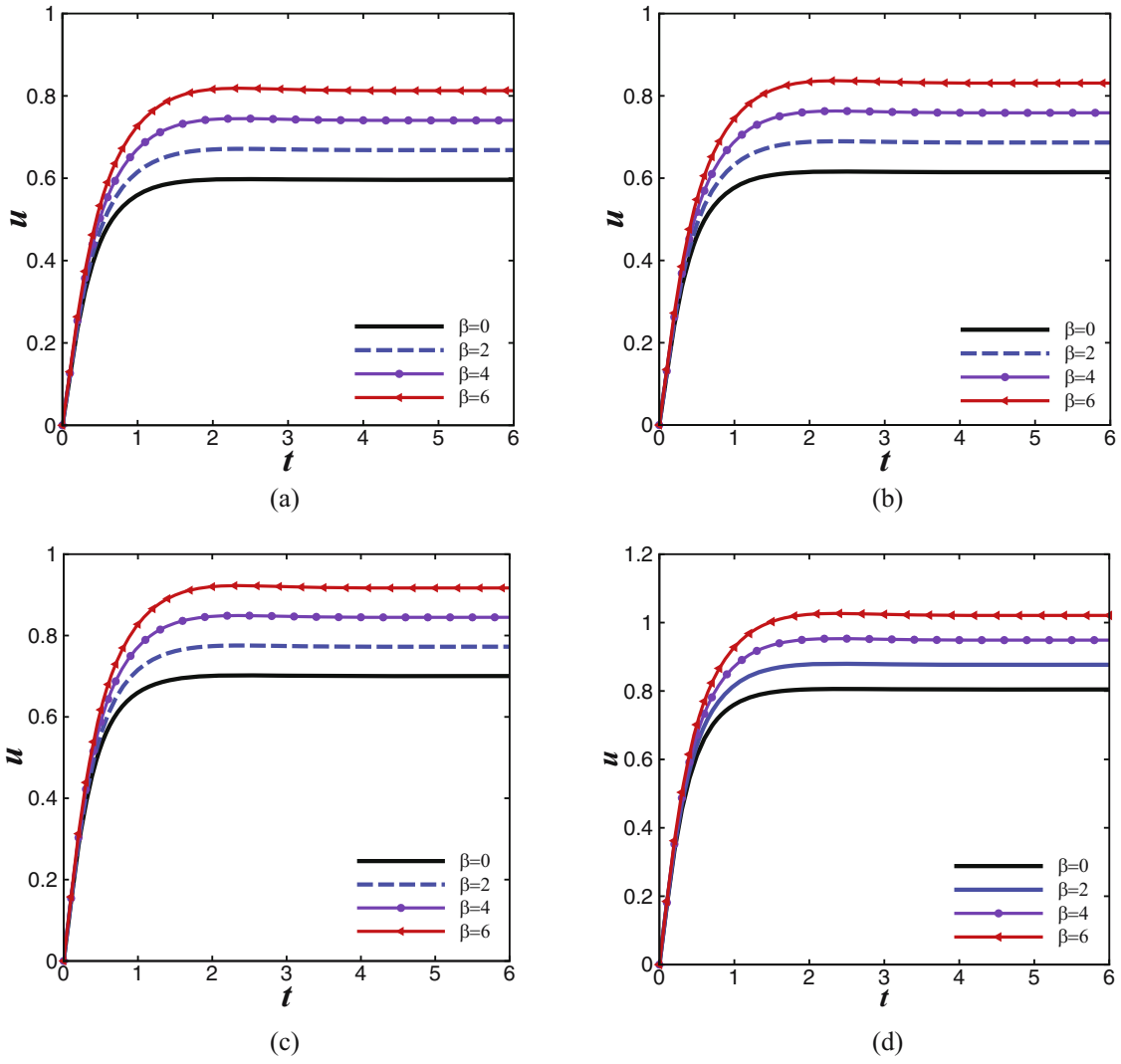

Figure 6: Effects of different β and ψ_0 on dimensionless velocity profiles ($\lambda_1 = 0.8$, $\lambda_2 = 0.3$, Ha = 1, $\Omega = 0$, $K = 20$, $x = 0.95$). (a) $\psi_0 = 1$, (b) $\psi_0 = 2$, (c) $\psi_0 = 5$, (d) $\psi_0 = 10$.

when the negative pressure gradient is greater ($\Omega = -10$) than the sum of the electroosmotic force and the Lorentz force, the fluid flows in the opposite direction (see Figure 7(a and b)). When the pressure gradient is constant, the velocity u increases with the increase of zeta potential ψ_0. The higher the zeta potential ψ_0 is, the larger the electroosmotic force is, and the forward driving force is larger than the reverse driving force, so the fluid flows in the positive direction. In conclusion, β and zeta potential ψ_0 have significant effects on dimensionless velocity u.

Figure 8 analyzes the effect of different relaxation time λ_1, retardation time λ_2 and wall zeta potential ψ_0 on dimensionless velocity profile at $x = 0.5$. As can be seen from Figure 8(a and b), with the increase of λ_1, the velocity distribution shows a large oscillation, this is because longer relaxation time implies greater elastic effect and smaller recovery capacity. Due to Jeffrey's "fading memory" phenomenon, the increased relaxation time makes the velocity profile more prone to change under the action of applied electric field. As can be seen from Figure 8(c and d), the amplitude of the velocity profile decreases with the increase of λ_2. This implies that the flow is subject to greater resistance with increase of retardation time λ_2 due to the suppression effect of the retardation time λ_2. Physically, larger retardation time corresponding to Jeffrey fluid makes it more viscous, resulting in less velocity amplitude. The velocity at $x = 0.5$ (i.e., outside of the EDL) remains unchanged with the multiplication of wall zeta potential ψ_0. The main reason is that there is no sufficient time for the flow diffusing far into the mid-plane of the wall, and velocity variation is restricted only within the EDL. In

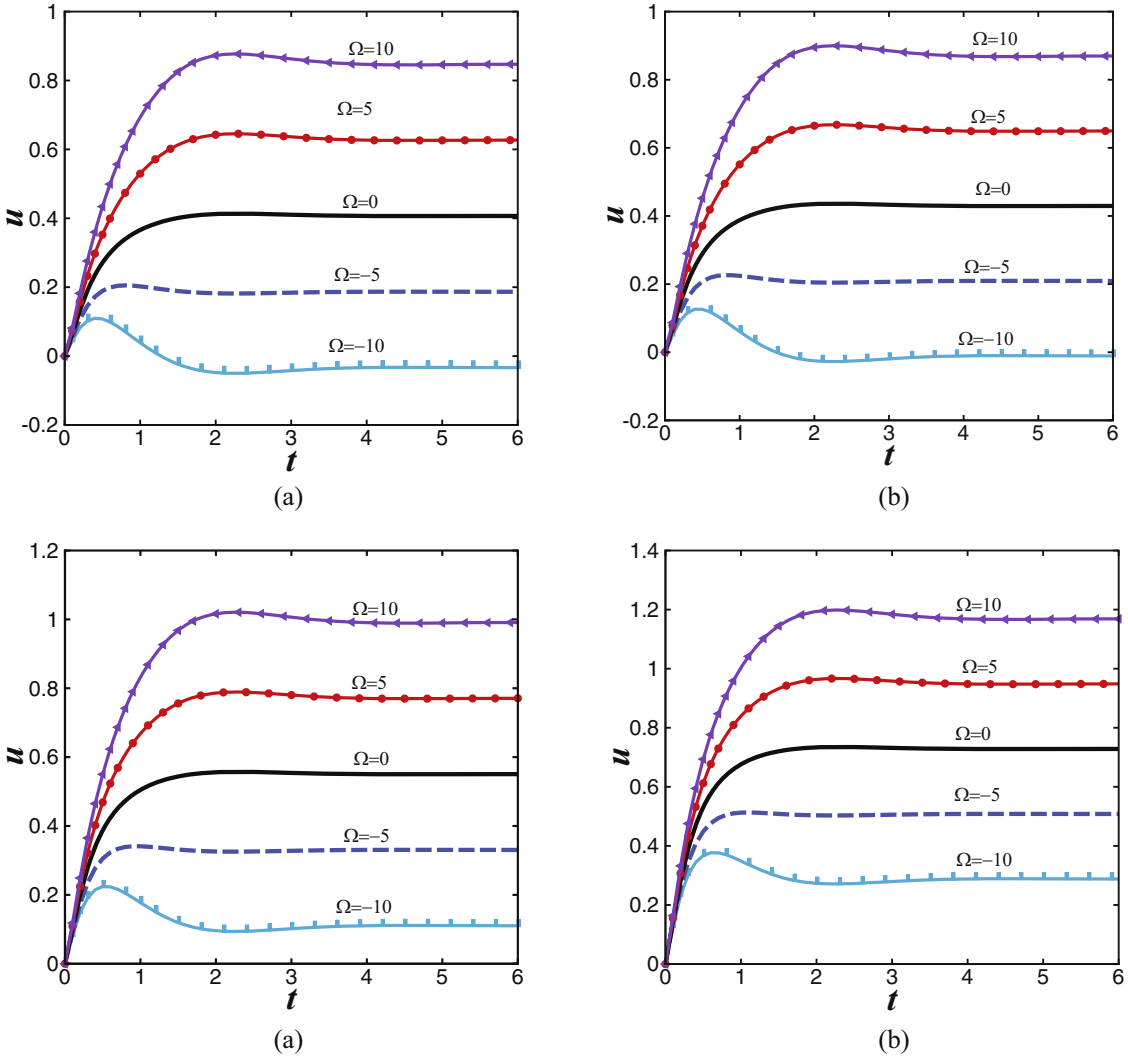

Figure 7: Effects of different Ω and ψ_0 on dimensionless velocity profiles ($\lambda_1 = 0.8, \lambda_2 = 0.3, \mathrm{Ha} = 0.5, \beta = 0, K = 10, x = 0.95$). (a) $\psi_0 = 1$, (b) $\psi_0 = 2$, (c) $\psi_0 = 5$, and (d) $\psi_0 = 10$.

addition, the fluid velocity reaches a steady state with the increase of time.

Figure 9 shows a comparison of dimensionless velocity amplitudes for Newtonian, Maxwell, and Jeffrey Fluids. As can be seen from Figure 9, the velocity amplitudes of Newtonian, Maxwell and Jeffrey fluids increase significantly at high zeta potential than that at low zeta potential. Therefore, the extension from low zeta potential to high zeta potential is necessary for the study of fluid flow in microchannels. In addition, it can also be seen physically from Figure 9 that the Maxwell fluid has larger velocity than those of Newtonian and Jeffrey fluids due to the shear thinning effect of the viscoelastic fluid. Shear thinning is an effect where viscosity decreases with the increasing rate of shear stress. Moreover, the Jeffrey fluid has smaller velocity than Newtonian and Maxwell fluids, because the effect of retardation suppresses the generation of the quick variation of the velocity.

6 Conclusion

The magnetofluid unsteady electroosmotic flow of Jeffrey fluid in parallel microchannels is studied in this work. In the absence of Debye–Hückel approximation, the nonlinear Poisson–Boltzmann equation, Cauchy-momentum equation and Jeffrey constitutive equation are solved by the finite difference method and the Chebyshev spectral method. By numerical computations, the influence of

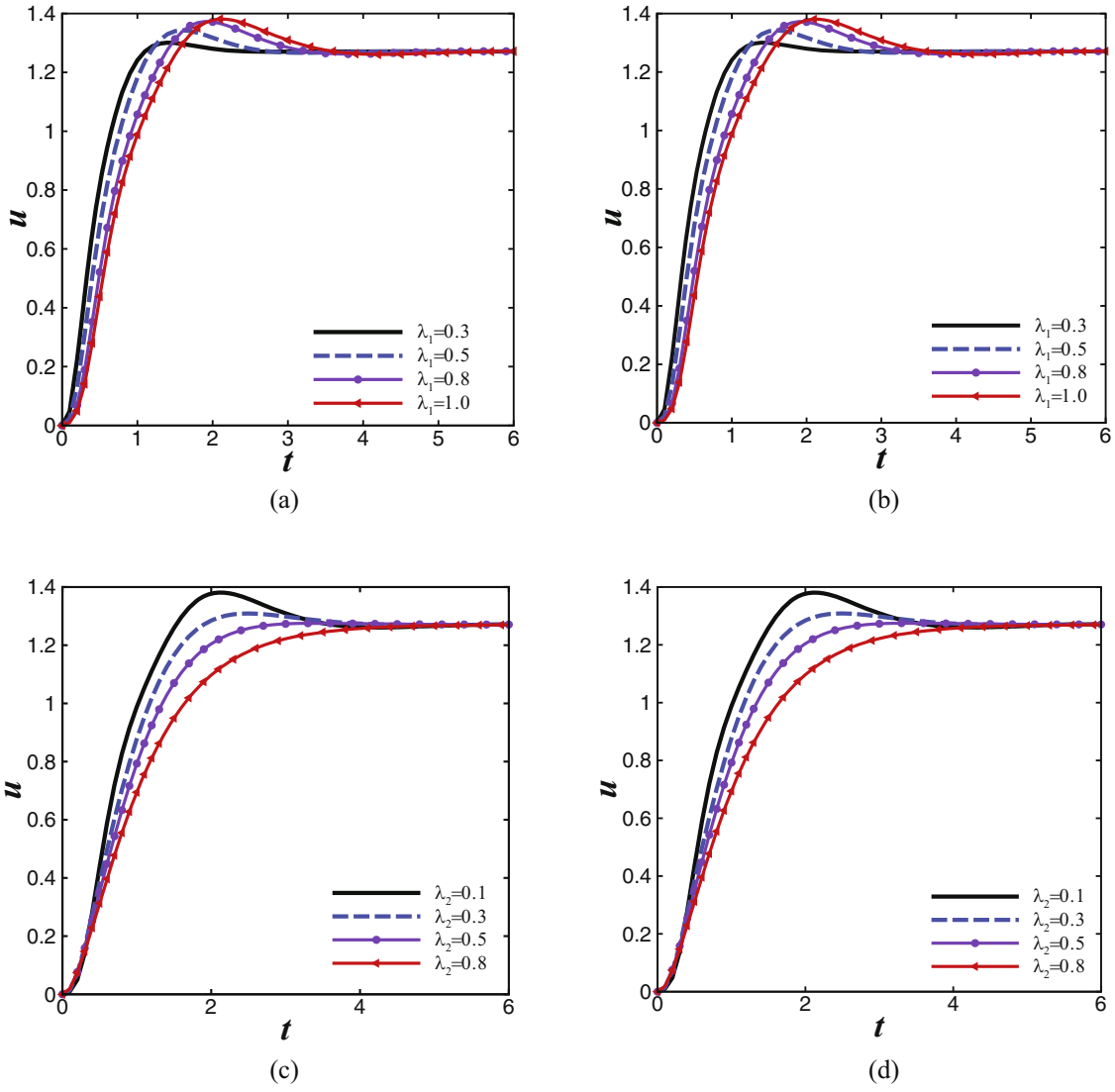

Figure 8: Effects of different relaxation times λ_1 and wall zeta potential ψ_0 on the dimensionless velocity profile (Ha = 1, β = 2, Ω = 0, K = 20, x = 0.5). (a) ψ_0 = 5, (b) ψ_0 = 10, (c) ψ_0 = 5, and (d) ψ_0 = 10.

Hartmann number Ha, wall zeta potential ψ_0, relaxation time λ_1 and retardation time λ_2, dimensionless electric field intensity in z axial direction β, the ratio of axial pressure gradient, and electroosmotic drive velocity Ω on the velocity distribution is presented. The following conclusions are drawn.

1) The finite difference method and the Chebyshev spectral method are effective methods to solve the potential and velocity distribution of microfluidic under high zeta potential, and Chebyshev spectral method has higher accuracy and less calculation.
2) With the increase of wall zeta potential ψ_0, the magnitude of the velocity amplitude u increases, and the maximum variation area of velocity u is concentrated on the EDL.
3) When Ha < 1, the velocity u increases with the increase of Ha. However, when Ha increases to a certain value, the velocity u decreases with the increase of Ha.
4) The velocity profile of Jeffrey fluid increases as dimensionless electric field intensity β in z axial direction increases.
5) The positive pressure gradient (Ω > 0) promotes the flow of the fluid and the reverse pressure gradient (Ω < 0) impedes the flow of the fluid.
6) The oscillation amplitude of velocity distribution increases with the increase of relaxation time λ_1 and decreases with the increase of retardation time λ_2. The velocity u gradually becomes stable with the change of time.
7) The velocity amplitude of Newtonian fluid, Maxwell fluid, and Jeffrey fluid at high zeta potential is

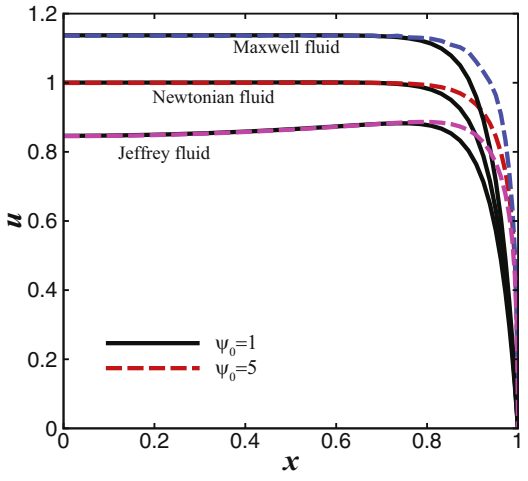

Figure 9: Comparison of the velocity amplitudes for Newtonian, Maxwell, and Jeffrey fluids (Ha = 1, β = 1, Ω = 0, K = 20, t = 2). For Newtonian fluid: λ_1 = 0, λ_2 = 0; for Maxwell fluid: λ_1 = 1, λ_2 = 0 and for Jeffrey fluid: λ_1 = 1, λ_2 = 0.8.

significantly higher than that at low zeta potential, so it is of great significance to study the influence of high zeta potential on fluid characteristics.

Acknowledgments: The author wishes to express his appreciation to the anonymous reviewers for their high-level comments and the kind editors for all their assistance.

Funding information: This work was supported by the National Natural Science Foundation of China (Approval Nos. 12062018, 12172333), Program for Young Talents of Science and Technology in Universities of Inner Mongolia Autonomous Region (Approval No. NJYT22075), and the Natural Science Foundation of Inner Mongolia (Approval No. 2020MS01015).

Author contributions: All authors have accepted responsibility for the entire content of this manuscript and approved its submission.

Conflict of interest: The authors state no conflict of interest.

References

[1] Rong CW, Papadopoulos KD. Electroosmotic flow through porous media: cylindrical and annular models. Colloids Surf A Physicochem Eng Asp. 2000;161(3):469–47.

[2] Chang CC, Chang YW. Starting electroosmotic flow in an annulus and in a rectangular channel. Electrophoresis. 2010;29(14):2970–9.

[3] Afonso AM, Alves MA, Pinho FT. Analytical solution of mixed electro-osmotic pressure driven flows of viscoelastic fluids in microchannels. J Non-Newton Fluid. 2009;159(1–3):50–63.

[4] Matin MH, Ohshima H. Thermal transport characteristics of combined electroosmotic and pressure driven flow in soft nanofluidics. J Colloid Interface Sci. 2016;476:167–76.

[5] Moatimid GM, Mohamed MAA, Hassan MA, El-Dakdoky EMM. Electro-osmotic flow and heat transfer of a non-Newtonian nanofluid under the influence of peristalsis. Pramana-J Phys. 2019;92:90.

[6] Tan Z, Liu J. Electro-osmotic flow of Eyring fluids in a circular microtube with Navier's slip boundary condition. Phys Lett. 2017;381(32):2573–7.

[7] Liu QS, Yang LG, Su J. Transient electroosmotic flow of general Jeffrey fluid between two micro-parallel plates. Acta Phys Sin. 2013;62(14):1691–702.

[8] Shamshuddin MD, Mishra SR, Thumma T. Chemically reacting radiative Casson fluid over an inclined porous plate: a numerical study. In: Srinivasacharya D, Srinivas Reddy R. (eds). Numer Heat Transfer Fluid Flow. Singapore: Springer; 2019, p. 469–79.

[9] Shamshuddin MD, Ibrahim W. Finite element numerical technique for magneto-micropolar nanofluid flow filled with chemically reactive casson fluid between parallel plates subjected to rotatory system with electrical and Hall currents. Int J Simul Model. 2021;42:1–20. doi: 10.1080/02286203.2021.2012634.

[10] Shahid A, Huang HL, Khalique CM, Bhatti MM. Numerical analysis of activation energy on MHD nanofluid flow with exponential temperature-ependent viscosity past a porous plate. J Therm Anal Calorim. 2021;143(3):2585–96.

[11] Chakraborty S, Paul D. Microchannel flow control through a combined electromagnetohydrodynamic transport. J Phys D. 2006;39(24):5364–71.

[12] Ganguly S, Sarkar S, Hota TK, Mishra M. Thermally developing combined electroosmotic and pressure-driven flow of nanofluids in a microchannel under the effect of magnetic field. Chem Eng Sci. 2015;126:10–21.

[13] Zhao GP, Jian YJ, Li FQ. Streaming potential and heat transfer of nanofluids in microchannels in the presence of magnetic field. J Magn Magn Mater. 2016;407:75–82.

[14] Das S, Chakraborty S, Mitra SK. Magnetohydrodynamics in narrow fluidic channels in presence of spatially non-uniform magnetic fields: framework for combined magnetohydrodynamic and magnetophoretic particle transport. Microfluid Nanofluidics. 2012;13(5):799–807.

[15] Jian YJ. Transient MHD heat transfer and entropy generation in a microparallel channel combined with pressure and electroosmotic effects. Int J Heat Mass Transf. 2015;89:193–205.

[16] Wang X. The unsteady electroosmotic flow of the Jeffrey fluid between micro-parallel plates under a vertical magnetic field [dissertation]. Hohhot: Inner Mongolia University; 2015.

[17] Yang CH. Study on the flow and heat transfer characteristic of electroosmosis under the action of magnetic field [dissertation]. Hohhot: Inner Mongolia University; 2020.

[18] Liu QS, Jian YJ, Yang LG. Alternating current electroosmotic flow of the Jeffreys fluids through a slit microchannel. Phys Fluids. 2011;23:102001.
[19] Yang X, Qi HT, Jiang XY. Numerical analysis for electroosmotic flow of fractional Maxwell fluids. Appl Math Comput. 2018;78:1–8.
[20] Vasu N, De S. Electroosmotic flow of power-law fluids at high zeta potentials. Colloids Surf A Physicochem Eng Asp. 2010;368(1–3):44–52.
[21] Xie ZY, Jian YJ. Rotating electroosmotic flow of power-law fluids at high zeta potentials. Colloids Surf A Physicochem Eng Asp. 2014;461:231–9.
[22] Chang L, Jian YJ. Time periodic electroosmotic flow of the generalized Maxwell fluids between two micro-parallel plates with high zeta potential. Acta Phys Sin-CH ED. 2012;61(12):124702.
[23] Chen HH, Liu QS. Rotating electro-osmotic flow at high zeta potentials in a microchannel. J Inner Mongolia Univ (Natural Sci Ed). 2018;49(2):135–43.
[24] Ram MS, Shamshuddin MD, Spandana K. Numerical simulation of stagnation point flow in magneto micropolar fluid over a stretchable surface under influence of activation energy and bilateral reaction. Int Commun Heat Mass Transf. 2021;129:105679.
[25] Ram MS, Shravani K, Shamshuddin MD, Salawu SO. Investigation of porosity significance on an Oldroyd-B fluid flow transport between parallel plates: Closed form solution. Heat Transfer. 2022;51:658–76.
[26] Rajput GR, Shamshuddin MD, Salawu SO. Thermosolutal convective non-Newtonian radiative Casson fluid transport over a vertical plate propagated by Arrhenius kinetics with heat source/sink. Heat Transfer. 2021;50(3):2829–48.
[27] Ahmed F. Fully developed forced convective Jeffrey fluid flow through concentric pipes annular duct. Eur Phys J Plus. 2021;136:12.
[28] Shahzad F, Jamshed W, Koulali A, Aissa A, Safdar R, Akgül EK, et al. Computational examination of Jeffrey nanofluid through a stretchable surface employing Tiwari and Das model. Open Phys. 2021;19:897–911.
[29] Li DS, Ma L, Dong JY, Li K. Time-periodic pulse electroosmotic flow of Jeffreys fluids through a microannulus. Open Phys. 2021;19(1):867–76.
[30] Gireesha BJ, Umeshaiah MD, Prasannakumara BC, Shashikumar NS, Archana M. Impact of nonlinear thermal radiation on magnetohydrodynamic three-dimensional boundary layer flow of jeffrey nanofluid over a nonlinearly permeable stretching sheet. Physica A: Stat Mech Applic. 2020;549:124051.
[31] Bird RB, Stewart WE, Lightfoot EN. Transport phenomena. 2nd edn. New York: John Wiley and Sons, Inc; 2001.
[32] Zhang X. Efficient solution of MATLAB differential equations: principle and implementation of spectral method. Beijing: Machinery Industry Press; 2016.
[33] Guo W, Labrosse G, Narayanan R. The application of the Chebyshev-spectral method in transport phenomena. Berlin Heidelberg: Springer-Verlag; 2012. p. 68.
[34] Humane PP, Patil VS, Patil AB, Shamshuddin MD, Rajput GR. Dynamics of multiple slip boundaries effect on MHD Casson-Williamson double-diffusive nanofluid flow past an inclined magnetic stretching sheet. Proc IMechE E J Process Mechanical Eng. 2022;236:1–21.
[35] Jang J, Lee SS. Theoretical and experimental study of MHD (magnetohydrodynamic) micropump. Sensors Actuators. 2000;80(1):84–9.